

Cosmological constraints on small-scale primordial non-Gaussianity

Jing-Zhi Zhou^{1,*}, Zhi-Chao Li^{1,†} and Di Wu^{2,‡}

¹*Center for Joint Quantum Studies and Department of Physics,
School of Science, Tianjin University, Tianjin 300350, China*

²*School of Fundamental Physics and Mathematical Sciences, Hangzhou Institute for Advanced Study,
University of Chinese Academy of Sciences, Hangzhou 310024, China*

In contrast to the large-scale primordial power spectrum $\mathcal{P}_\zeta(k)$ and primordial non-Gaussianity f_{NL} , which are strictly constrained, the small-scale $\mathcal{P}_\zeta(k)$ and f_{NL} remain less restricted. Considering local-type primordial non-Gaussianity, we study the primordial black holes (PBHs) and scalar induced gravitational waves (SIGWs) caused by large-amplitude small-scale primordial power spectrum. By analyzing current observational data from pulsar timing array (PTA), cosmic microwave background (CMB), baryon acoustic oscillations (BAO), and abundance of PBHs, and combining them with the signal-to-noise ratio (SNR) analysis of Laser Interferometer Space Antenna (LISA), we rigorously constrain the parameter space of $\mathcal{P}_\zeta(k)$ and f_{NL} . Furthermore, we examine the effects of different shapes of the primordial power spectrum on these constraints and comprehensively calculate the Bayes factors for various models. Our results indicate that SIGWs generated by a monochromatic primordial power spectrum are more likely to dominate current PTA observations, with the corresponding constraint on the primordial non-Gaussian parameter being $-10.0 < f_{NL} < 1.2$.

I. INTRODUCTIONS

Our universe originated from primordial perturbations generated during the inflationary era [1–3]. These primordial perturbations carry the physical information from the inflationary period, influencing all subsequent evolutionary processes of the universe [4–8]. Through current cosmological observations on different scales, we can determine the physical properties of primordial perturbations on various scales, providing us with crucial information on new physics during the evolution of the universe [9–16].

Over the past few decades, cosmological research has made significant strides [17–19]. The cosmological observations, such as cosmic microwave background (CMB), large scale structure (LSS), Big-Bang nucleosynthesis (BBN), and baryon acoustic oscillations (BAO), provide us with a wealth of precise cosmological data, enabling us to accurately determine the physical properties of primordial perturbations [20–26]. Specifically, on large scales ($\gtrsim 1$ Mpc), the power spectrum of primordial curvature perturbations is approximately a scale-invariant spectrum, with an amplitude $A_\zeta \approx 2 \times 10^{-9}$ [27]. Moreover, the current constraint on the tensor-to-scalar ratio r is $r < 0.064$ at 95% confidence level [28]. Furthermore, as one of the most important properties of primordial perturbations, the non-Gaussianity of the primordial power spectrum on large scales has also been tightly constrained. For instance, the current cosmological observations re-

veal that the parameter of local-type primordial non-Gaussianity $f_{NL} = -0.9 \pm 5.1$ at 68% confidence level [29]. However, unlike large-scale primordial perturbations, there are no strict observational constraints on small-scale ($\lesssim 1$ Mpc) primordial perturbations [30]. Exploring how to leverage different cosmological observations to constrain the small-scale primordial power spectrum and its associated non-Gaussianity represents one of the foremost challenges in further cosmological research.

Various inflationary models can generate primordial curvature perturbations with significant amplitudes and non-Gaussianity on small scales. Examples include multi-field inflation models [31–36], Higgs inflation models [31–36], and inflation models based on modified gravity theories [37–43]. Constraining the primordial curvature perturbations and their associated non-Gaussianity on small scales requires taking into account their impact on small-scale cosmological observables. More precisely, after inflation ends and these large amplitude primordial perturbations re-enter the horizon, they will cause substantial density perturbations that collapse to form primordial black holes (PBHs) [44–55]. This process will also inevitably generate scalar induced gravitational waves (SIGWs) [56–59]. By analyzing the abundance of PBHs and the observations of SIGWs such as Laser Interferometer Space Antenna (LISA) and pulsar timing array (PTA), we can identify the parameter space for the small-scale primordial power spectrum $\mathcal{P}_\zeta(k)$ and the associated parameter of local-type primordial non-Gaussianity f_{NL} allowed by current observations.

In this paper, we concentrate on the constraints imposed by current cosmological observations on small-scale local-type primordial non-Gaussianity.

* zhoujingzhi@tju.edu.cn

† lizc@tju.edu.cn

‡ wudi@ucas.ac.cn

Specifically, we consider the following observational constraints:

1, PTA observations [60–68]: we assume that SIGWs dominate the current PTA observations and utilize the PTA data to perform the Bayesian analysis on the parameter space of $\mathcal{P}_\zeta(k)$ and f_{NL} . By combining the model where supermassive black hole binaries (SMBHBs) dominate PTA observations, we calculate the Bayes factors between different models, thereby rigorously analyzing the feasibility of each model in dominating PTA observations.

2, Large-scale cosmological observations [69–72]: large-scale cosmological observations such as CMB, BAO, and BBN have provided an upper limit on the energy density of SIGWs ρ_{GW} . Using this upper limit, we can constrain the parameter space of $\mathcal{P}_\zeta(k)$ and f_{NL} .

3, LISA [73–75]: In scenarios where different models dominate PTA observations, we rigorously analyze the signal-to-noise ratio (SNR) of LISA. This allows us to determine whether the high-frequency regions of the corresponding energy density spectra of gravitational waves (GWs) can be observed in the LISA band.

4, Abundance of PBHs [76]: Given the specific form of $\mathcal{P}_\zeta(k)$ and f_{NL} , we can calculate the abundance of primordial black holes f_{PBH} and require $f_{PBH} < 1$, thus constraining the parameter space of $\mathcal{P}_\zeta(k)$ and f_{NL} .

Using the aforementioned four types of cosmological observations, we can rigorously quantify the constraints on the small-scale primordial power spectrum and primordial non-Gaussianity.

This paper is organized as follows. In Sec. II, we study the energy density spectra of SIGWs and analyze the constraints on $\mathcal{P}_\zeta(k)$ and f_{NL} imposed by PTA, LISA, and large-scale cosmological observations. In Sec. III, we calculate the abundance of PBHs and examine the impact of PBH abundance on the constraints of f_{NL} . In Sec. IV, we investigate the impact of various forms of the primordial power spectrum on the constraints of f_{NL} . Additionally, we compute the Bayes factors between different models using the current PTA data. Finally, we summarize

our results and give some discussions in Sec. V.

II. SCALAR INDUCED GRAVITATIONAL WAVES

In June 2023, the PTA collaborations NANOGrav [60], EPTA [62], PPTA [61], and the CPTA [63] reported positive evidence for an isotropic, stochastic background of GWs within the nHz frequency range. As mentioned in ref. [64], among the numerous potential contributors to the stochastic gravitational wave background (SGWB), SIGWs show the highest Bayes factor, which makes them one of the most likely dominant sources. In this case, considering the scenario where SIGWs dominate the current nHz frequency band of the SGWB, we perform a Bayesian analysis using the current PTA observational data. This allows us to determine the current PTA constraints on small-scale primordial power spectrum $\mathcal{P}_\zeta(k)$ and the corresponding parameter of local-type primordial non-Gaussianity f_{NL} [77–80].

In the case of the local-type primordial non-Gaussianity, the non-Gaussian primordial curvature perturbation can be expressed as a local perturbative expansion around the Gaussian primordial curvature perturbation. In momentum space, the primordial curvature perturbation can be written as [56, 81]

$$\zeta_{\mathbf{k}}^{ng} = \zeta_{\mathbf{k}}^g + \frac{3}{5} f_{NL} \int \frac{d^3n}{(2\pi)^{3/2}} \zeta_{\mathbf{k}-\mathbf{n}}^g \zeta_{\mathbf{n}}^g , \quad (1)$$

where \mathbf{n} is the three dimensional momentum variable. $\zeta_{\mathbf{k}}^g$ is the Gaussian primordial curvature perturbation.

The second-order SIGWs can be expressed as

$$h_{\mathbf{k}}^{\lambda,(2)}(\eta) = \int \frac{d^3p}{(2\pi)^{3/2}} \varepsilon^{\lambda,lm}(\mathbf{k}) p_l p_m I^{(2)} \zeta_{\mathbf{k}-\mathbf{p}} \zeta_{\mathbf{p}} , \quad (2)$$

where $\varepsilon^{\lambda,lm}(\mathbf{k}) (\lambda = +, \times)$ are polarization tensors. The explicit expressions of the second-order kernel functions $I^{(2)}$ can be found in Ref. [82]. By analyzing the two-point correlation function of second-order SIGWs, we can determine the corresponding energy density spectrum. The calculation of the two-point correlation function $\langle h_{\mathbf{k}}^{\lambda,(2)} h_{\mathbf{k}'}^{\lambda',(2)} \rangle$ involves the four-point correlation function associated with primordial curvature perturbations: $\langle \zeta_{\mathbf{k}-\mathbf{p}} \zeta_{\mathbf{p}} \zeta_{\mathbf{k}'-\mathbf{p}'} \zeta_{\mathbf{p}'} \rangle$. Combining the expression of local-type non-Gaussian primordial curvature perturbations provided in Eq. (1), the total energy density spectrum of second-order SIGWs can be written as [83, 84]

$$\begin{aligned} \bar{\Omega}_{GW}^{(2)}(k) = & \bar{\Omega}_{GW}^G + \bar{\Omega}_{GW}^H + \bar{\Omega}_{GW}^C + \bar{\Omega}_{GW}^Z \\ & + \bar{\Omega}_{GW}^R + \bar{\Omega}_{GW}^P + \bar{\Omega}_{GW}^N , \end{aligned} \quad (3)$$

where the energy density spectrum of the second-order SIGWs is categorized into seven distinct loop diagram contributions. In Eq. (3), the contributions of Gaussian one-loop diagrams, proportional to A_ζ^2 , are denoted by $\bar{\Omega}_{\text{GW}}^G$. The symbols $\bar{\Omega}_{\text{GW}}^H$, $\bar{\Omega}_{\text{GW}}^C$, and $\bar{\Omega}_{\text{GW}}^Z$ denote non-Gaussian contributions of two-loop diagrams proportional to $A_\zeta^3 (f_{\text{NL}})^2$. The symbols $\bar{\Omega}_{\text{GW}}^R$, $\bar{\Omega}_{\text{GW}}^P$, and $\bar{\Omega}_{\text{GW}}^N$ correspond to non-Gaussian contributions of three-loop diagrams proportional to $A_\zeta^4 (f_{\text{NL}})^4$. The explicit expressions of these loop diagrams of second-order SIGWs in Eq. (3) can be found in Ref. [85].

Furthermore, due to the significant primordial perturbations on small scales, higher-order cosmological perturbations significantly affect the total energy density spectrum of SIGWs, thus modifying the parameter space of $\mathcal{P}_\zeta(k)$ and f_{NL} determined by PTA observations. Specifically, the third-order SIGWs can be expressed as [86, 87]

$$h_{\mathbf{k}}^{\lambda,(3)}(\eta) = \sum_{i=1}^4 h_{i,\mathbf{k}}^{\lambda,(3)}(\eta) = \int \frac{d^3 p}{(2\pi)^{3/2}} \int \frac{d^3 q}{(2\pi)^{3/2}} \times \varepsilon^{\lambda,lm}(\mathbf{k}) \mathbb{P}_{lm}^i I_i^{(3)} \zeta_{\mathbf{k}-\mathbf{p}} \zeta_{\mathbf{p}-\mathbf{q}} \zeta_{\mathbf{q}}, \quad (4)$$

where the momentum polynomials $\mathbb{P}_{lm}^i (i = 1, 2, 3, 4)$ are given by

$$\mathbb{P}_{lm}^1 = q_m (p_l - q_l), \quad \mathbb{P}_{lm}^2 = \Lambda_{lm}^{rs}(\mathbf{p}) q_r q_s, \quad (5)$$

$$\mathbb{P}_{lm}^3 = (\mathcal{T}_m^r(\mathbf{p}) p_l + \mathcal{T}_l^r(\mathbf{p}) p_m) \frac{p^s}{p^2} q_r q_s, \quad (6)$$

$$\mathbb{P}_{lm}^4 = p_l p_m. \quad (7)$$

In Eq. (5), $\Lambda_{ij}^{lm}(\mathbf{p})$ represents the transverse and traceless operator, defined as

$$\Lambda_{ij}^{lm}(\mathbf{p}) = \mathcal{T}_i^l(\mathbf{p}) \mathcal{T}_j^m(\mathbf{p}) - \frac{1}{2} \mathcal{T}_{ij}(\mathbf{p}) \mathcal{T}^{lm}(\mathbf{p}), \quad (8)$$

where $\mathcal{T}_{ij}(\mathbf{p}) = \delta_{ij} - p_i p_j / p^2$. In Eq. (4), the contribution of third-order SIGWs consists of four parts, denoted as $h_{i,\mathbf{k}}^{\lambda,(3)} (i = 1, 2, 3, 4)$. They correspond respectively to the third-order gravitational waves directly induced by first-order scalar perturbations, and to the third-order gravitational waves jointly induced by first-order scalar perturbations and three types of second-order perturbations. The explicit expressions of the third-order kernel functions $I_i^{(3)} (i = 1, 2, 3, 4)$ in Eq. (4) are provided in Ref. [86].

When we consider SIGWs up to the third order, the two-point correlation function of the gravitational waves can be expressed as

$$\langle h_{\mathbf{k}}^\lambda h_{\mathbf{k}'}^{\lambda'} \rangle = \langle h_{\mathbf{k}}^{\lambda,(2)} h_{\mathbf{k}'}^{\lambda',(2)} \rangle + \langle h_{\mathbf{k}}^{\lambda,(3)} h_{\mathbf{k}'}^{\lambda',(3)} \rangle + 2 \langle h_{\mathbf{k}}^{\lambda,(3)} h_{\mathbf{k}'}^{\lambda',(2)} \rangle. \quad (9)$$

Here, we have ignored the potential large-amplitude primordial gravitational waves on small scales [88–90]. As previously discussed, in Eq. (9), $\langle h_{\mathbf{k}}^{\lambda,(2)} h_{\mathbf{k}'}^{\lambda',(2)} \rangle$ represents the two-point correlation function of second-order SIGWs, proportional to the four-point correlation function of primordial curvature perturbations: $\langle \zeta_{\mathbf{k}-\mathbf{p}} \zeta_{\mathbf{p}} \zeta_{\mathbf{k}'-\mathbf{p}'} \zeta_{\mathbf{p}'} \rangle$. Similarly, the two-point correlation function of third-order SIGWs $\langle h_{\mathbf{k}}^{\lambda,(3)} h_{\mathbf{k}'}^{\lambda',(3)} \rangle$ is proportional to the six-point correlation function of primordial curvature perturbations: $\langle \zeta_{\mathbf{k}-\mathbf{p}} \zeta_{\mathbf{p}-\mathbf{q}} \zeta_{\mathbf{q}} \zeta_{\mathbf{k}'-\mathbf{p}'} \zeta_{\mathbf{p}'-\mathbf{q}'} \zeta_{\mathbf{q}'} \rangle$. And the cross-correlation function $\langle h_{\mathbf{k}}^{\lambda,(3)} h_{\mathbf{k}'}^{\lambda',(2)} \rangle$ is proportional to the five-point correlation function of primordial curvature perturbations: $\langle \zeta_{\mathbf{k}-\mathbf{p}} \zeta_{\mathbf{p}-\mathbf{q}} \zeta_{\mathbf{q}} \zeta_{\mathbf{k}'-\mathbf{p}'} \zeta_{\mathbf{p}'} \rangle$. In addition, the cross two-point correlation function $\langle h_{\mathbf{k}}^{\lambda,(3)} h_{\mathbf{k}'}^{\lambda',(2)} \rangle$ will only modify the total energy density spectrum of SIGWs if primordial non-Gaussianity is present. The lowest-order contribution of this modification is proportional to $A_\zeta^3 f_{\text{NL}}$, corresponding to the two-loop diagrams of SIGWs [91]. In summary, when considering SIGWs up to the third order, the corresponding one-loop ($\sim A_\zeta^2$) and two-loop ($\sim A_\zeta^3$) contributions can be expressed as

$$\bar{\Omega}_{\text{GW}}^{\text{tot}}(k) = \bar{\Omega}_{\text{GW}}^G + \bar{\Omega}_{\text{GW}}^H + \bar{\Omega}_{\text{GW}}^C + \bar{\Omega}_{\text{GW}}^Z + \bar{\Omega}_{\text{GW}}^{(3)}(k) + 2\bar{\Omega}_{\text{GW}}^{(3,2)}(k, \eta). \quad (10)$$

When $f_{\text{NL}} < 0$, the contributions of $\bar{\Omega}_{\text{GW}}^{(2,3)}$ can significantly suppress the total energy density spectrum of SIGWs. The explicit expressions of third-order corrections $\bar{\Omega}_{\text{GW}}^{(3)}$ and $\bar{\Omega}_{\text{GW}}^{(3,2)}$ can be found in Refs. [91, 92].

In this study, we focus on the following two types of energy density spectra:

1. The total energy density spectrum of second-order SIGWs as described in Eq. (3).
2. The complete one-loop and two-loop contributions involving up to third-order SIGWs as presented in Eq. (10).

Furthermore, Eq. (3) and Eq. (10) present the formulas for the energy density spectrum of SIGWs during the radiation-dominated (RD) era. Taking into account the thermal history of the universe, we obtain the current energy density spectrum [93]

$$\bar{\Omega}_{\text{GW},0}(k) = \Omega_{\text{rad},0} \left(\frac{g_{*,\rho,e}}{g_{*,\rho,0}} \right) \left(\frac{g_{*,s,0}}{g_{*,s,e}} \right)^{4/3} \bar{\Omega}_{\text{GW}}(k), \quad (11)$$

where $\Omega_{\text{rad},0}$ ($= 4.2 \times 10^{-5} h^{-2}$) is the energy density fraction of radiations today. The effect numbers of relativistic species $g_{*,\rho}$ and $g_{*,s}$ can be found in Ref. [94]. And the dimensionless Hubble constant is $h = 0.6736$ [27].

A. PTA observations

Given the specific form of the primordial power spectrum $\mathcal{P}_\zeta(k)$, we can calculate the energy density spectrum of SIGWs. In this section, we consider the log-normal (LN) primordial power spectrum

$$\mathcal{P}_\zeta^{\text{LN}}(k) = \frac{A_\zeta}{\sqrt{2\pi\sigma^2}} \exp\left(-\frac{1}{2\sigma^2} \ln^2(k/k_*)\right), \quad (12)$$

where A_ζ is the amplitude of primordial power spectrum and $k_* = 2\pi f_*$ is the wavenumber at which the primordial power spectrum has a LN peak. The parameter σ indicates the width of the LN primordial power spectrum.

To characterize the parameter space of $\mathcal{P}_\zeta^{\text{LN}}(k)$ and f_{NL} inferred from PTA observations, we construct the likelihood function using kernel density estimator (KDE) representations of the free spectra [95–97]. The likelihood is given by

$$\ln \mathcal{L}(d|\theta) = \sum_{i=1}^{N_f} p(\Phi_i, \theta). \quad (13)$$

Here $p(\Phi_i, \theta)$ represents the probability of Φ_i given the parameter θ , and $\Phi_i = \Phi(f_i)$ denotes the time delay

$$\Phi(f) = \sqrt{\frac{H_0^2 \Omega_{\text{GW}}(f)}{8\pi^2 f^5 T_{\text{obs}}}}, \quad (14)$$

where $H_0 = h \times 100 \text{ km/s/Mpc}$ is the present-day value of the Hubble constant. We directly use the KDEs representation of the first 14 frequency bins of the HD(Helling-Downs)-correlated free spectrum in NANOGrav 15-year dataset [98]. Bayesian analysis is performed by BILBY [99] with its built-in DYNESTY nested sampler [100, 101]. Furthermore, to investigate the impact of astrophysical sources of the SGWB on current PTA observations, we consider the SGWB generated by SMBHBs, with the corresponding energy density spectrum given by [64, 95]

$$\Omega_{\text{GW}}^{\text{BH}}(f) = \frac{2\pi^2 A_{\text{BHB}}^2}{3H_0^2 h^2} \left(\frac{f}{\text{year}^{-1}}\right)^{5-\gamma_{\text{BHB}}} \text{year}^{-2}. \quad (15)$$

Here, the prior distribution for $(\log_{10} A_{\text{BHB}}, \gamma_{\text{BHB}})$ follows a multivariate normal distribution [64], whose mean and covariance matrix are given by

$$\boldsymbol{\mu}_{\text{BHB}} = \begin{pmatrix} -15.6 \\ 4.7 \end{pmatrix}, \boldsymbol{\sigma}_{\text{BHB}} = 0.1 \begin{pmatrix} 2.8 & -0.026 \\ -0.026 & 2.8 \end{pmatrix}. \quad (16)$$

For the second-order SIGWs in Eq. (3), the posterior distributions are depicted in Fig. 1a, where the prior distributions of $\log(f_*/\text{Hz})$, $\log(A_\zeta)$, σ ,

and f_{NL} are uniformly distributed over the ranges $[-10, 3]$, $[-3, 1]$, $[0.1, 2.5]$, and $[-30, 30]$ respectively. The corresponding energy density spectra of second-order SIGWs are given in Fig. 2. Furthermore, to determine the impact of third-order SIGWs on the amplitude of the primordial power spectrum A_ζ , we calculate the energy density spectrum in Eq. (3) and Eq. (10), with the parameter σ fixed. Fig. 1b compares the corresponding posterior distributions, showing that the presence of third-order SIGWs significantly modifies the parameter space of A_ζ and f_{NL} determined by current PTA observations. More precisely, after taking into account the contributions of the third-order SIGWs, the blue curve of f_{NL} in Fig. 1b is no longer symmetric, and the parameter interval $f_{\text{NL}} \in [-10, -1]$ is significantly excluded. When $f_{\text{NL}} \in [-10, -1]$, the cross-correlation function $\langle h_{\mathbf{k}}^{\lambda, (3)}(\eta) h_{\mathbf{k}'}^{\lambda', (2)}(\eta) \rangle$ will suppress the total energy density spectrum, which prevents the total energy density spectrum of SIGWs from fitting well with the observational data of PTA in this parameter interval.

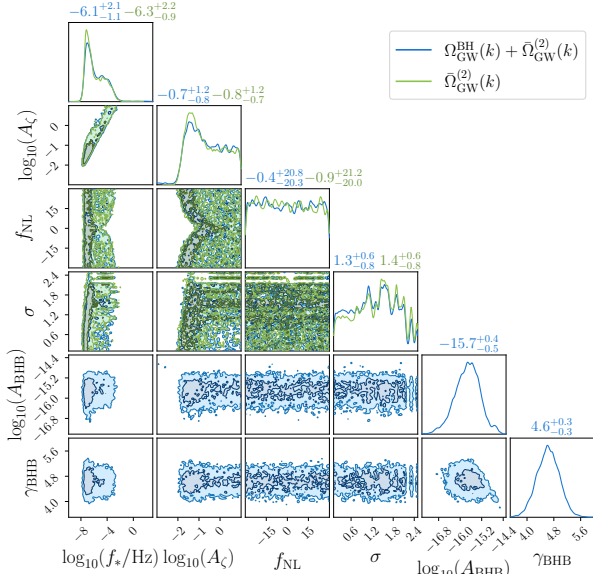
B. SNR of LISA

In scenarios where the high-frequency region of the energy spectrum of SIGWs is within detection range of LISA, we can combine PTA observational data to thoroughly analyze the impact of $\mathcal{P}_\zeta(k)$ and f_{NL} on the SNR of LISA, thereby determining the influence of the high-frequency SIGWs on LISA observations. The SNR ρ of LISA is given by [102]

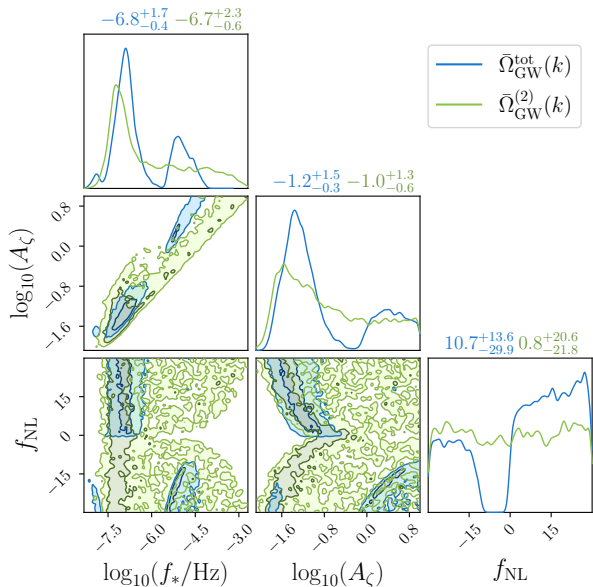
$$\rho = \sqrt{T} \left[\int df \left(\frac{\bar{\Omega}_{\text{GW},0}(f)}{\Omega_n(f)} \right)^2 \right]^{1/2}, \quad (17)$$

where T is the observation time and we set $T = 4$ years here. $\Omega_n(f) = 2\pi^2 f^3 S_n / 3H_0^2$, where H_0 is the Hubble constant and S_n is the strain noise power spectral density [103].

As shown in Fig. 3, we provide a two-dimensional distribution plot of SNR of LISA as a function of σ and f_* . The results indicate that when SIGWs dominate the current PTA observations, the corresponding energy density spectrum in the high-frequency region can influence observations in the LISA frequency band. Moreover, as elaborated in Sec. III B, large-amplitude primordial perturbations at small scales can lead to the formation of primordial black holes, while binary PBH mergers also contribute to the SGWB. When SIGWs dominate PTA observations, the SGWB produced by binary PBH mergers may also impact GW observations at higher frequencies.



(a) Posterior distributions of $\Omega_{\text{GW}}^{\text{BH}}(k) + \bar{\Omega}_{\text{GW}}^{(2)}(k)$ and $\bar{\Omega}_{\text{GW}}^{(2)}(k)$.



(b) Posterior distributions of $\bar{\Omega}_{\text{GW}}^{(2)}(k)$ and $\bar{\Omega}_{\text{GW}}^{\text{tot}}(k)$.

FIG. 1: The corner plot of the posterior distributions. The contours in the off-diagonal panels denote the 68% and 95% credible intervals of the 2D posteriors. The numbers above the figures represent the median values and 1- σ ranges of the parameters. (a): The blue and green solid curves correspond to the second-order SIGW energy spectrum in Eq. (3) with or without SMBHB. (b): The green and blue lines represent the energy density spectra of second-order SIGWs in Eq. (3) and the complete one-loop and two-loop energy spectra incorporating up to third-order SIGWs in Eq. (10), respectively. We have fixed $\sigma = 1$.

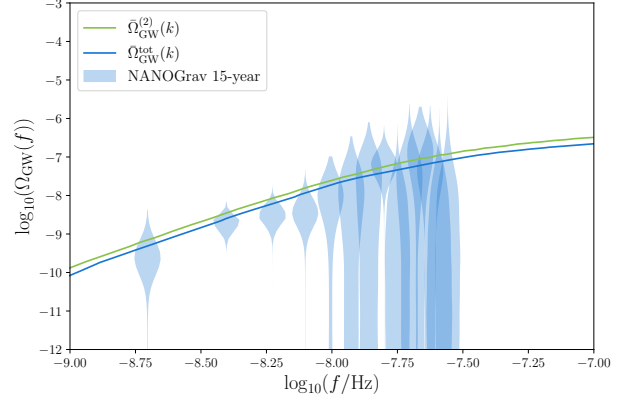


FIG. 2: The energy density spectra $\bar{\Omega}_{\text{GW}}^{(2)}(k)$ and $\bar{\Omega}_{\text{GW}}^{\text{tot}}(k)$ correspond to Fig. 1b. The energy density spectra derived from the free spectrum of the NANOGrav 15-year are shown with blue. The green curves represent the energy density spectra of GWs with different line styles labeled in the figure. Specifically, the parameters for the blue solid line are: $\log_{10}(A_\zeta) = -1.51$, $\log_{10}(f_*/\text{Hz}) = -7.14$, and $f_{\text{NL}} = 22.3$; and for the green solid line, the parameters are: $\log_{10}(A_\zeta) = -1.32$, $\log_{10}(f_*/\text{Hz}) = -6.991$, and $f_{\text{NL}} = 23.4$. These parameters are selected based on the maximum a posterior (MAP) estimate for each parameter.

C. Constraints from large-scale cosmological observations

Besides the direct observation of the energy density spectrum of SIGWs, SIGWs can serve as an additional radiation component, affecting the large-scale cosmological observations [69, 71, 106]. More precisely, the total energy density of SIGWs satisfies

$$h^2 \rho_{\text{GW}} = \int_{f_{\min}}^{\infty} h^2 \Omega_{\text{GW},0}(k) d(\ln k) < 2.9 \times 10^{-7} \quad (18)$$

at 95% confidence level for CMB+BAO data [107]. It should be noted that the large-scale cosmological observation constraints in Ref. [107] are stronger than the constraints obtained from the relativistic degrees of freedom N_{eff} in Refs. [69, 72]. More precisely, taking into account only the constraints from N_{eff} , the energy density spectrum of SIGWs satisfies $h^2 \rho_{\text{GW}} < 2.11 \times 10^{-6}$ at the 95% confidence level, which represents a weaker constraint compared to that provided in Eq. (18). In Fig. 4, we present the parameter space of $\mathcal{P}_\zeta(k)$ and f_{NL} determined by Eq. (18).

As depicted in Fig. 4, the total energy density spectrum of second-order SIGWs $\Omega_{\text{GW}}^{(2)}$ in Eq. (3) is proportional to $A_\zeta^2 + (f_{\text{NL}})^2 A_\zeta^3 + (f_{\text{NL}})^4 A_\zeta^4$, creating

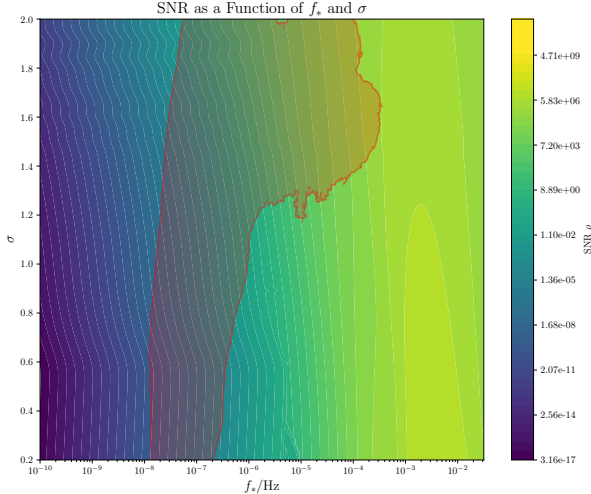


FIG. 3: The SNR of LISA as a function of f_* and σ . The heatmap shows the SNR for second-order SIGW energy spectrum $\bar{\Omega}_{\text{GW}}^{(2)}(k)$ with fixed values of $A_\zeta = 0.1$ and $f_{\text{NL}} = 5$. The red shading represents the 68% credible interval corresponding to the two-dimensional posterior distribution of $\bar{\Omega}_{\text{GW}}^{(2)}(k)$ shown in Fig. 1a, obtained using the KDE method implemented in ChainConsumer [104, 105].

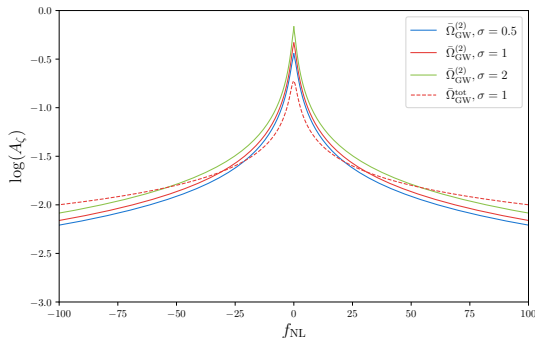


FIG. 4: The upper limits of the amplitude of LN primordial power spectrum A_ζ as determined by large-scale observations under different non-Gaussian parameter f_{NL} . The figure illustrates the upper limits of A_ζ , as determined by the energy density spectra of Eq. (3) (solid line) and Eq. (10) (dashed line).

a degeneracy for opposite values of f_{NL} , where the upper limits of A_ζ for f_{NL} and $-f_{\text{NL}}$ are identical. However, in Eq. (10), where one-loop and two-loop contributions extend to third order, the corresponding energy density spectrum $\Omega_{\text{GW}}^{\text{tot}}$ is proportional to $A_\zeta^2 + A_\zeta^3 + f_{\text{NL}} A_\zeta^3 + (f_{\text{NL}})^2 A_\zeta^3$, causing the upper limits of A_ζ to differ for parameters f_{NL} with equal magnitudes but opposite signs. Furthermore, when $|f_{\text{NL}}|$

is small, the third-order SIGWs contribution from Eq. (10) suppresses the upper bound of A_ζ . As $|f_{\text{NL}}|$ increases, the three-loop contribution proportional to $(f_{\text{NL}})^4 A_\zeta^4$ in Eq. (3) grows, leading to the upper limit of A_ζ from Eq. (3) becoming lower than that from Eq. (10).

III. PRIMORDIAL BLACK HOLES

On small scales, large-amplitude primordial curvature perturbations can generate SIGWs upon re-entering the horizon after inflation. This process is inevitably accompanied by the formation of PBHs. In this section, we consider PBHs formed from large-amplitude primordial curvature perturbations on small scales, and the constraints they impose on the small-scale primordial power spectrum and primordial non-Gaussianity. Furthermore, binary PBH mergers will also generate an additional SGWB [93]. By combining the results of SIGWs from the previous section, we analyze the impact of binary PBH mergers on the observations of SGWB.

A. Abundance of PBHs

The abundance of PBHs can be expressed as [46]

$$f_{\text{pbh}} \simeq 2.5 \times 10^8 \beta \left(\frac{g_*^{\text{form}}}{10.75} \right)^{-\frac{1}{4}} \left(\frac{m_{\text{pbh}}}{M_\odot} \right)^{-\frac{1}{2}}. \quad (19)$$

We consider an approximate formula for f_{PBH} in Eq. (19). The corresponding rigorous expressions are provided in Refs. [108–110]. The mass of PBH is characterised by the scaling law relation

$$\begin{aligned} M_{\text{PBH}} &= \mathcal{K} M_H (\mathcal{C} - \mathcal{C}_{\text{th}})^\gamma, \\ M_H &\approx 17 M_\odot \left(\frac{k}{10^6 \text{Mpc}^{-1}} \right)^{-2} \left(\frac{g_*}{10.75} \right)^{-1/6}, \end{aligned} \quad (20)$$

where the threshold \mathcal{C}_{th} have been studied in Ref. [111]. The compaction function $\mathcal{C} = \mathcal{C}_1 - \mathcal{C}_1^2/(4\Phi)$ can be obtained from the linear $\mathcal{C}_1 = \mathcal{C}_G dF/d\zeta_G$ component, that uses $\mathcal{C}_G = -2\Phi r \zeta'_G$, where $\Phi = 3(1+w)/(5+3w)$. In the case of local-type primordial non-Gaussianity, $F(\zeta_G) = \zeta_G + \frac{3}{5} f_{\text{NL}} \zeta_G^2$. We set $\mathcal{K} = 4.4$ and $\gamma = 0.38$ [109, 112]. The mass fraction β can be obtained by integrating the probability distribution function

$$\beta = \int_{\mathcal{D}} \mathcal{K} (\mathcal{C} - \mathcal{C}_{\text{th}})^\gamma P_G(\mathcal{C}_G, \zeta_G) d\mathcal{C}_G d\zeta_G, \quad (21)$$

where the domain of integration in Eq. (21) is $\mathcal{D} = \{\mathcal{C}(\mathcal{C}_G, \zeta_G) > \mathcal{C}_{\text{th}} \wedge \mathcal{C}_1(\mathcal{C}_G, \zeta_G) < 2\Phi\}$. In Eq. (21),

the Gaussian components are distributed as

$$P_G(\mathcal{C}_G, \zeta_G) = \frac{e^{-\left[\frac{1}{2(1-\gamma_{cr}^2)}\left(\frac{\mathcal{C}_G}{\sigma_c} - \frac{\gamma_{cr}\zeta_G}{\sigma_r}\right)^2 - \frac{\zeta_G^2}{2\sigma_r^2}\right]}}{2\pi\sigma_c\sigma_r\sqrt{1-\gamma_{cr}^2}}. \quad (22)$$

The correlators in Eq. (22) are given by

$$\begin{aligned} \sigma_c^2 &= \frac{4\Phi^2}{9} \int_0^\infty \frac{dk}{k} (kr_m)^4 W^2(k, r_m) P_\zeta^T, \\ \sigma_{cr}^2 &= \frac{2\Phi}{3} \int_0^\infty \frac{dk}{k} (kr_m)^2 W(k, r_m) W_s(k, r_m) P_\zeta^T, \\ \sigma_r^2 &= \int_0^\infty \frac{dk}{k} W_s^2(k, r_m) P_\zeta^T, \end{aligned} \quad (23)$$

where $P_\zeta^T = T^2(k, r_m) P_\zeta(k)$, and $\gamma_{cr} \equiv \sigma_{cr}^2 / \sigma_c \sigma_r$. Here, we have defined $W(k, r_m)$, $W_s(k, r_m)$ and $T(k, r_m)$ as the top-hat window function, the spherical-shell window function, and the radiation transfer function [113]. It is important to note that the calculation of PBHs abundance is highly model-dependent, and different models can lead to significant variations in the estimated abundance [109].

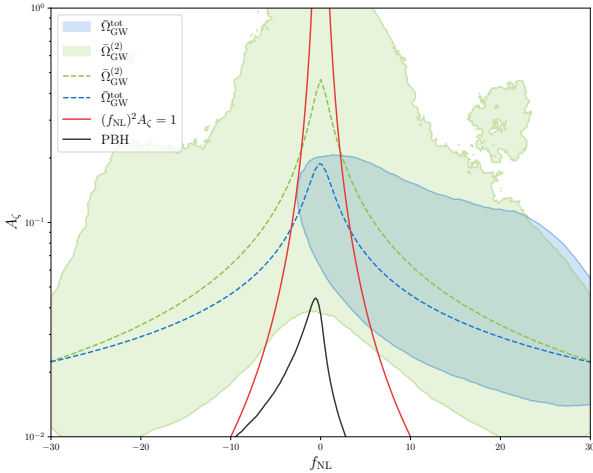


FIG. 5: The constraints on A_ζ and f_{NL} assuming the LN primordial power spectrum. The blue and green shaded regions represent the 68% credible intervals corresponding to the two-dimensional posterior distribution shown in Fig. 1b with the KDE method. The blue and green dashed lines indicate the upper bounds on the amplitude A_ζ shown in Fig. 4. The red curve corresponds to the relation $(f_{NL})^2 A_\zeta = 1$. The black line corresponds to the PBH abundance constraint given in Ref. [76].

As shown in Fig. 5, we present the constraints on the amplitude of the small-scale primordial power spectrum A_ζ and the primordial non-Gaussian parameter f_{NL} in the case of the LN primordial power spectrum, based on current

CMB+BAO+PTA+PBHs observations. Furthermore, in the case of local-type primordial non-Gaussianity, the second-order energy density $\bar{\Omega}_{GW}^{(2)}$ is proportional to $A_\zeta^2 + (f_{NL})^2 A_\zeta^3 + (f_{NL})^4 A_\zeta^4$, and each increase in the non-Gaussian order introduces an additional perturbative expansion coefficient $(f_{NL})^2 A_\zeta$. This result holds for n -th order SIGWs, such that: $\bar{\Omega}_{GW}^{(n)} \sim A_\zeta^n \sum_{m=0}^n (f_{NL})^{2m} A_\zeta^m$. Therefore, the necessary condition for ensuring the convergence of the perturbative expansion of non-Gaussian contributions is $(f_{NL})^2 A_\zeta < 1$. This theoretical constraint corresponds to the region below the red curve in Fig. 5.

In summary, the parameter space allowed by current observations corresponds to the region below the curves in Fig. 5. When SIGWs dominate the current PTA observations, the parameters f_{NL} and A_ζ must also reside within the blue or green shaded regions in Fig. 5.

Through various types of cosmological observations across different scales, we can effectively constrain the primordial non-Gaussian parameter f_{NL} on small scales. It is important to note that these constraints depend on the specific form of the small-scale primordial power spectrum. In Sec. IV, we will analyze the impact of different primordial power spectra on the constraints of the parameter f_{NL} . Additionally, the parameter space shown in Fig. 5 is influenced by experimental observations, and future high-precision cosmological measurements will further refine our ability to constrain small-scale primordial non-Gaussian parameter.

B. SGWB from binary PBH mergers

In Sec. II B, we investigated how SIGWs influence the SNR of LISA. As we previously mentioned, when SIGWs dominate PTA observations, their generation inevitably accompanies the formation of PBHs, and binary PBH mergers also contribute to the SGWB. In this paper, we follow the formation scenario of PBH binaries proposed in Refs. [114–116]. Based on the merger rate of the PBH binaries, we can calculate the energy density spectra $\Omega_{GW}^{PBH}(f)$ of the corresponding SGWB. For the SGWB produced by binary PBH mergers, $\Omega_{GW}^{PBH}(f)$ can be expressed as

$$\Omega_{GW}^{PBH}(f) = \frac{\nu}{\rho_c} \int_0^{\frac{f_{cut}}{f}-1} \frac{R_{PBH}(z)}{(1+z)H(z)} \frac{dE_{GW}}{df_s} (f_s) dz, \quad (24)$$

where the explicit expressions of $\frac{dE_{\text{GW}}}{df_s}(f_s)$ and $R_{\text{PBH}}(z)$ can be found in Ref. [93]. As shown in Fig. 6, when SIGWs lie within the observational frequency range of PTA, the SGWB generated by the corresponding binary PBH mergers falls within LISA's detection frequency band, which may affect the SNR of LISA.

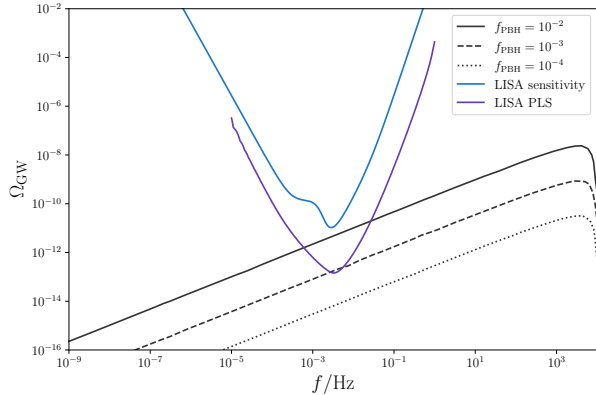


FIG. 6: The energy density spectrum $\bar{\Omega}_{\text{GW}}^{\text{PBH}}(k)$ in Eq. (24). The black curves represent the energy spectra of $\Omega_{\text{GW}}^{\text{PBH}}(k)$ with $M_{\text{PBH}} = 1M_\odot$ and $f_{\text{PBH}} = 10^{-2}$ (solid), 10^{-3} (dashed) and 10^{-4} (dotted) [117]. The blue curve and the purple curve represent the standard LISA sensitivity and the power law sensitivity (PLS) [118] with SNR = 10.

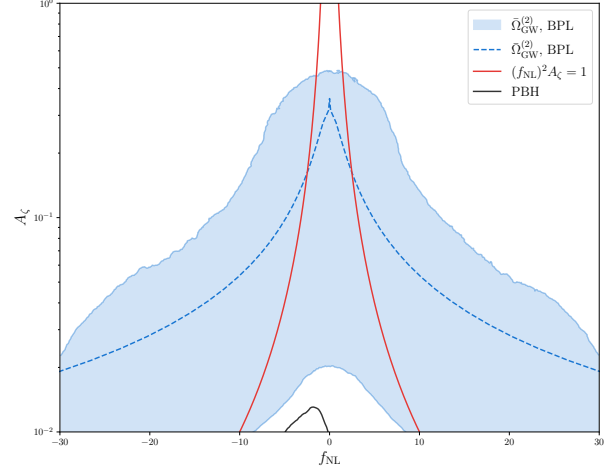
IV. SHAPE OF THE PRIMORDIAL POWER SPECTRA

In the above discussion, we have provided the constraints on the local-type non-Gaussian parameter f_{NL} from current cosmological observations for a LN primordial power spectrum. This result depends on the specific form of the primordial power spectrum. To study the effects of different shapes of the primordial power spectrum on small-scale cosmological observations, we need to combine current PTA observational data and analyze the Bayes factors of different primordial power spectra. Besides the previously analyzed LN primordial power spectrum, we consider the broken power-law (BPL) primordial power spectrum [119, 120]

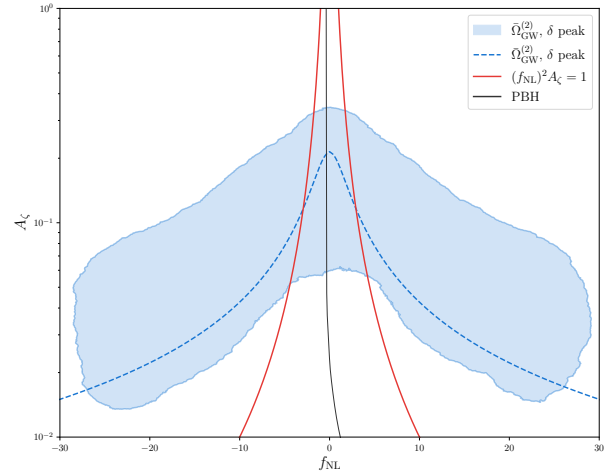
$$\mathcal{P}_\zeta^{\text{BPL}}(k) = \frac{A_\zeta(\alpha + \beta)}{\left(\beta(k/k_*)^{-\alpha} + \alpha(k/k_*)^\beta\right)}, \quad (25)$$

and the δ (monochromatic) primordial power spectrum [121–123]

$$\mathcal{P}_\zeta^\delta(k) = A_\zeta k_* \delta(k - k_*) . \quad (26)$$



(a) The constraints on A_ζ and f_{NL} assuming the BPL primordial power spectrum..



(b) The constraints on A_ζ and f_{NL} assuming the monochromatic primordial power spectrum.

FIG. 7: The constraints on A_ζ and f_{NL} assuming different primordial power spectrum. The blue shaded regions represent the 68% credible intervals corresponding to the two-dimensional posterior distribution with KDE method. The blue dashed lines indicate the upper bounds on the amplitude A_ζ from CMB+BAO data. The red curve corresponds to the relation $(f_{\text{NL}})^2 A_\zeta = 1$. The black line corresponds to the PBH abundance constraint given in Ref. [76]. As stated in Ref. [108], Eq. (21) is not applicable to a monochromatic primordial power spectrum. Therefore, we adopt the approach proposed in Ref. [124] to calculate the PBH abundance under the monochromatic primordial power spectrum scenario.

Similar to the discussions in Sec. II and Sec. III, the constraints imposed by current cosmological observations on the parameter space of the BPL primordial power spectrum and the monochromatic primordial power spectrum are presented in Fig. 7a and Fig. 7b, respectively. The corresponding posterior distributions are given in the Appendix A. For the monochromatic power spectrum, the prior distributions of $\log(f_*/\text{Hz})$, $\log(A_\zeta)$, and f_{NL} are uniformly distributed over the ranges $[-10, -5]$, $[-3, 0]$, and $[-30, 30]$ respectively. For the BPL power spectrum, the prior distributions of $\log(f_*/\text{Hz})$, $\log(A_\zeta)$, α , β and f_{NL} are uniformly distributed over the ranges $[-10, -5]$, $[-3, 0]$, $[1, 3]$, $[1, 3]$, and $[-30, 30]$ respectively.

To rigorously quantify the probability of different models dominating current PTA observations, we employ the Bayes factor to compare them. Specifically, the Bayes factor is defined as $B_{i,j} = \frac{Z_i}{Z_j}$, where Z_i represents the evidence of model H_i . Fig. 8 illustrates Bayes factors for comparisons between various models and the SMBHB model. As shown in Fig. 8, the Bayes factor analysis indicates that SIGWs generated by the monochromatic primordial power spectrum are more likely to dominate the current PTA observations.

In Table I, we summarize the main results of this section. The observational constraints on the parameter of small-scale primordial non-Gaussianity f_{NL} depend not only on the specific form of the primordial power spectrum but also on its amplitude A_ζ . In Table I, we have set $A_\zeta = 10^{-2}$. Note that the above conclusion differs from the constraints on f_{NL} at large scales, as the primordial power spectrum at large scales has already been strictly constrained by large-scale cosmological observations. Therefore, different forms of the primordial power spectrum do not need to be considered when determining the constraints on f_{NL} at large scales.

Furthermore, if no specific assumption is made about the origin of the SGWB in the PTA frequency band, the energy density spectrum of second-order SIGWs must not exceed the observed energy density spectrum in the PTA band. In this scenario, current PTA observations can still serve as an upper bound on the energy density spectrum of second-order SIGWs. Thus, when we require SIGWs to dominate the current PTA observations, the parameter space of f_{NL} and A_ζ must not only satisfy other cosmological constraints but also lie within the blue-shaded regions in Fig. 7a and Fig. 7b. Since $\bar{\Omega}_{\text{GW}}^{(2)}(k)$ increases with f_{NL} and A_ζ , if we do not assume that SIGWs dominate the SGWB in the PTA frequency band, then the value of A_ζ for a given f_{NL} must not exceed the blue-shaded regions in Fig. 7a and Fig. 7b.

	f_{NL}	Bayes factors
LN	$-9.5 < f_{\text{NL}} < 2.9$	23.75
BPL	$-5.0 < f_{\text{NL}} < -0.1$	22.61
δ peak	$-10.0 < f_{\text{NL}} < 1.2$	53.84
SMBHB	\times	1

TABLE I: Constraints from current cosmological observations on small-scale local-type non-Gaussian parameters. We set $A_\zeta = 1$.

Moreover, as discussed in Sec. II, the cross-correlation function $\langle h_{\mathbf{k}}^{\lambda, (3)} h_{\mathbf{k}'}^{\lambda', (2)} \rangle \sim f_{\text{NL}} A_\zeta^3$ can impact the results in Table I. When constraining the parameter f_{NL} using the energy density spectrum in Eq. (10), the current PTA observations cannot be dominated by SIGWs. As indicated by the blue shaded region in Fig. 5, the presence of the cross-correlation function $\langle h_{\mathbf{k}}^{\lambda, (3)} h_{\mathbf{k}'}^{\lambda', (2)} \rangle$ suppresses the total energy density spectrum of SIGWs when f_{NL} is negative, thus excluding certain parameter regions based on cosmological constraints. In this scenario, insisting that SIGWs dominate the current PTA observations would contradict the upper bound on the primordial black hole abundance.

V. CONCLUSION AND DISCUSSION

To study the constraints imposed by current cosmological observations on the small-scale primordial power spectrum $\mathcal{P}_\zeta(k)$ and the local-type non-Gaussian parameter f_{NL} , we analyzed the impact of large-amplitude small-scale primordial curvature perturbations, which induce the formation of PBHs and corresponding second-order SIGWs, on current cosmological observations at different scales. Future, more precise observations from PTA, PBHs, and large-scale cosmological observations will enable us to more tightly constrain the parameter space of $\mathcal{P}_\zeta(k)$ and f_{NL} . Furthermore, since SIGWs and PBHs abundance depend on the shape of the primordial power spectrum, we studied the impact of different primordial power spectra on the constraints of the parameter space and rigorously analyzed the Bayes factors of different models. Moreover, the constraints on f_{NL} imposed by current cosmological observations for different forms of the primordial power spectrum are summarized in Table I. The constraints on f_{NL} presented in Table I depend on the specific form and the amplitude of the primordial power spectra.

In this study, we evaluated the influence of second-order and third-order SIGWs on current cosmological observations. As shown in Refs. [125–129],

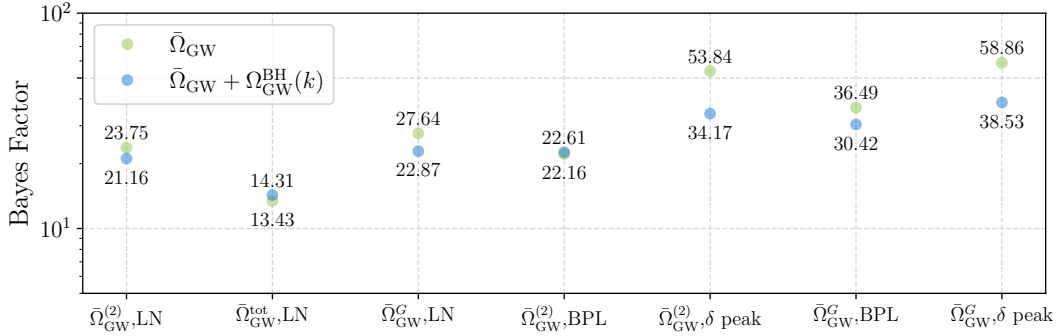


FIG. 8: The Bayes factors between different models. The vertical axis represents the Bayes factor of different models relative to SMBHB, and the horizontal axis represents the different models. The green dots are for models without SMBHB and the blue dots are for models in combination with the SMBHB signal.

second-order density perturbations induced by primordial perturbations will have a significant impact on the threshold δ_c and probability distribution function $P(\delta)$ of PBHs. When studying the large-amplitude primordial perturbations on small scales, the effects of higher-order cosmological perturbations cannot be ignored [130]. In addition to the influence of higher-order corrections, several other effects could impact the parameter space of $\mathcal{P}_\zeta(k)$ and f_{NL} . These include the effects of different dominant era of universe [131–133], the impact of large-amplitude small-scale primordial tensor perturbations [134–138], and interactions between SIGWs and matter [139–142]. The impact of these physical effects on the constraints of primordial non-Gaussianity might be systematically investigated in future research.

ACKNOWLEDGMENTS

This work has been funded by the National Nature Science Foundation of China under grant No. 12447127.

Appendix A: Posterior distributions

Based on the theoretical results of the energy density spectrum of second-order SIGWs, we present the posterior distributions determined by current PTA observations under different forms of the primordial power spectrum. As shown in Fig. 8, we further analyze the impact of SIGWs on PTA observations

when $f_{NL} = 0$. The posterior distributions for different models are provided in Fig. 9 ~ Fig. 14.

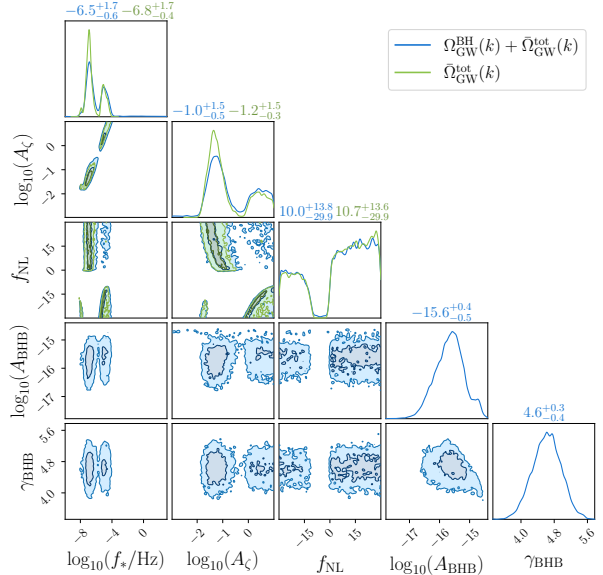


FIG. 9: Posterior distributions of $\bar{\Omega}_{GW}^{tot}(k)$ and $\bar{\Omega}_{GW}^{BH}(k) + \bar{\Omega}_{GW}^{tot}(k)$ with LN primordial power spectrum. The contours in the off-diagonal panels denote the 68% and 95% credible intervals of the 2D posteriors. The numbers above the figures represent the median values and 1- σ ranges of the parameters.

[1] D. H. Lyth and Y. Rodriguez, *Phys. Rev. Lett.* **95**, 121302 (2005), arXiv:astro-ph/0504045.

[2] S. Weinberg, *Phys. Rev. D* **72**, 043514 (2005), arXiv:hep-th/0506236.

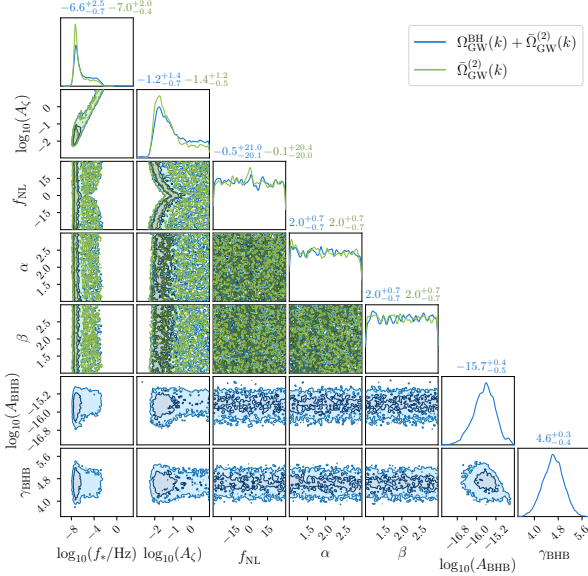


FIG. 10: Posterior distributions of $\bar{\Omega}_{\text{GW}}^{(2)}(k)$ and $\bar{\Omega}_{\text{GW}}^{\text{BH}}(k) + \bar{\Omega}_{\text{GW}}^{(2)}(k)$ with BPL primordial power spectrum. The contours in the off-diagonal panels denote the 68% and 95% credible intervals of the 2D posteriors. The numbers above the figures represent the median values and 1- σ ranges of the parameters.

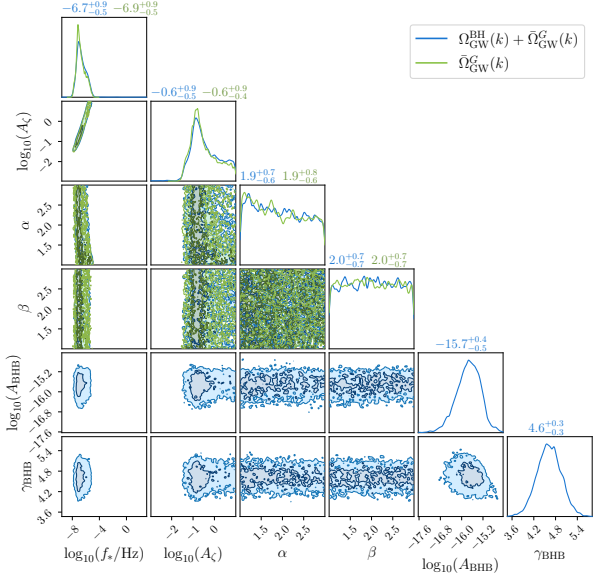


FIG. 11: Posterior distributions of $\bar{\Omega}_{\text{GW}}^G(k)$ and $\bar{\Omega}_{\text{GW}}^{\text{BH}}(k) + \bar{\Omega}_{\text{GW}}^G(k)$ with BPL primordial power spectrum. The contours in the off-diagonal panels denote the 68% and 95% credible intervals of the 2D posteriors. The numbers above the figures represent the median values and 1- σ ranges of the parameters.

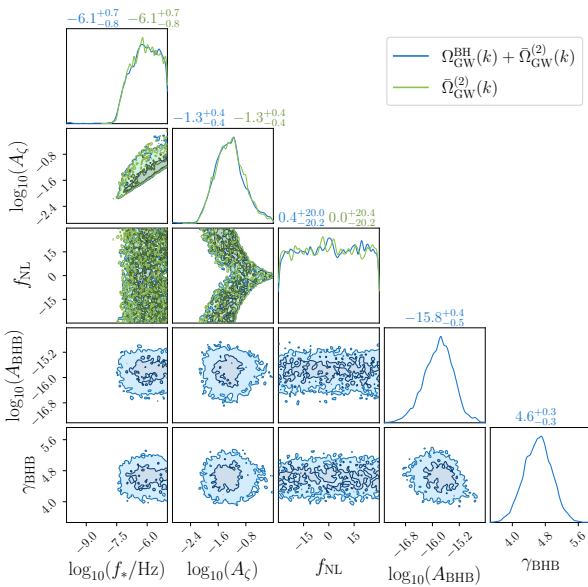


FIG. 12: Posterior distributions of $\bar{\Omega}_{\text{GW}}^{(2)}(k)$ and $\bar{\Omega}_{\text{GW}}^{\text{BH}}(k) + \bar{\Omega}_{\text{GW}}^{(2)}(k)$ with monochromatic primordial power spectrum. The contours in the off-diagonal panels denote the 68% and 95% credible intervals of the 2D posteriors. The numbers above the figures represent the median values and 1- σ ranges of the parameters.

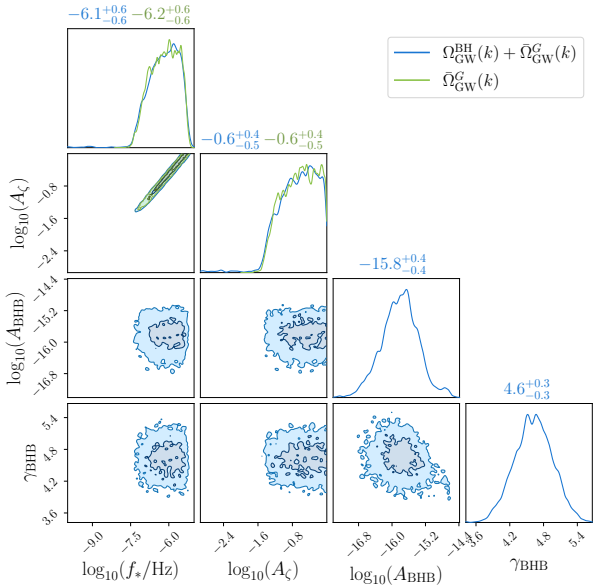


FIG. 13: Posterior distributions of $\bar{\Omega}_{\text{GW}}^G(k)$ and $\bar{\Omega}_{\text{GW}}^{\text{BH}}(k) + \bar{\Omega}_{\text{GW}}^G(k)$ with monochromatic primordial power spectrum. The contours in the off-diagonal panels denote the 68% and 95% credible intervals of the 2D posteriors. The numbers above the figures represent the median values and 1- σ ranges of the parameters.

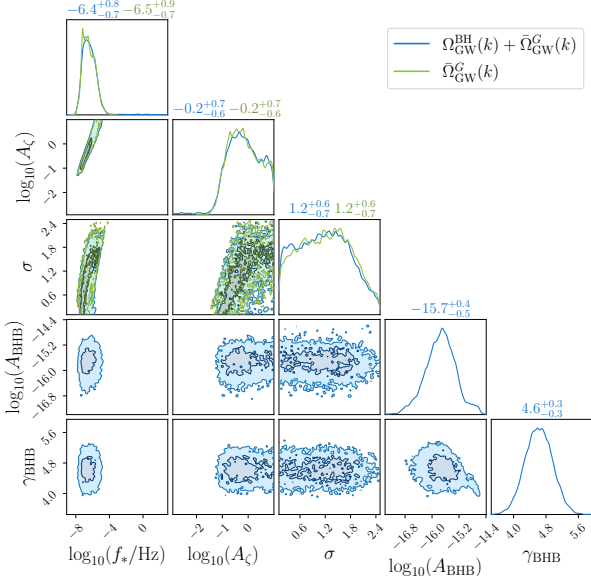


FIG. 14: Posterior distributions of $\bar{\Omega}_{\text{GW}}^G(k)$ and $\bar{\Omega}_{\text{GW}}^{\text{BH}}(k) + \bar{\Omega}_{\text{GW}}^G(k)$ with LN primordial power spectrum. The contours in the off-diagonal panels denote the 68% and 95% credible intervals of the 2D posteriors. The numbers above the figures represent the median values and 1- σ ranges of the parameters.

- [3] B. A. Bassett, S. Tsujikawa, and D. Wands, *Rev. Mod. Phys.* **78**, 537 (2006), arXiv:astro-ph/0507632.
- [4] D. Baumann, in *Theoretical Advanced Study Institute in Elementary Particle Physics: Physics of the Large and the Small* (2011) pp. 523–686, arXiv:0907.5424 [hep-th].
- [5] A. Riotto, *ICTP Lect. Notes Ser.* **14**, 317 (2003), arXiv:hep-ph/0210162.
- [6] D. S. Goldwirth and T. Piran, *Phys. Rept.* **214**, 223 (1992).
- [7] K. A. Malik and D. Wands, *Phys. Rept.* **475**, 1 (2009), arXiv:0809.4944 [astro-ph].
- [8] D. Baumann, *PoS TASI2017*, 009 (2018), arXiv:1807.03098 [hep-th].
- [9] I. G. Irastorza and J. Redondo, *Prog. Part. Nucl. Phys.* **102**, 89 (2018), arXiv:1801.08127 [hep-ph].
- [10] Y.-F. Cai, S. Capozziello, M. De Laurentis, and E. N. Saridakis, *Rept. Prog. Phys.* **79**, 106901 (2016), arXiv:1511.07586 [gr-qc].
- [11] D. J. E. Marsh, *Phys. Rept.* **643**, 1 (2016), arXiv:1510.07633 [astro-ph.CO].
- [12] A. De Felice and S. Tsujikawa, *Living Rev. Rel.* **13**, 3 (2010), arXiv:1002.4928 [gr-qc].
- [13] M. Bojowald, *Living Rev. Rel.* **8**, 11 (2005), arXiv:gr-qc/0601085.
- [14] M. Gasperini and G. Veneziano, *Phys. Rept.* **373**, 1 (2003), arXiv:hep-th/0207130.
- [15] D. H. Lyth and A. Riotto, *Phys. Rept.* **314**, 1 (1999), arXiv:hep-ph/9807278.
- [16] J. E. Kim and G. Carosi, *Rev. Mod. Phys.* **82**, 557 (2010), [Erratum: Rev.Mod.Phys. 91, 049902 (2019)], arXiv:0807.3125 [hep-ph].
- [17] E. Abdalla *et al.*, *JHEAp* **34**, 49 (2022), arXiv:2203.06142 [astro-ph.CO].
- [18] R. L. Workman *et al.* (Particle Data Group), *PTEP* **2022**, 083C01 (2022).
- [19] S. Navas *et al.* (Particle Data Group), *Phys. Rev. D* **110**, 030001 (2024).
- [20] F. Bernardeau, S. Colombi, E. Gaztanaga, and R. Scoccimarro, *Phys. Rept.* **367**, 1 (2002), arXiv:astro-ph/0112551.
- [21] N. Bartolo, E. Komatsu, S. Matarrese, and A. Riotto, *Phys. Rept.* **402**, 103 (2004), arXiv:astro-ph/0406398.
- [22] P. A. R. Ade *et al.* (Planck), *Astron. Astrophys.* **571**, A24 (2014), arXiv:1303.5084 [astro-ph.CO].
- [23] P. A. R. Ade *et al.* (Planck), *Astron. Astrophys.* **594**, A17 (2016), arXiv:1502.01592 [astro-ph.CO].
- [24] K. S. Dawson *et al.* (eBOSS), *Astron. J.* **151**, 44 (2016), arXiv:1508.04473 [astro-ph.CO].
- [25] N. Aghanim *et al.* (Planck), *Astron. Astrophys.* **641**, A1 (2020), arXiv:1807.06205 [astro-ph.CO].
- [26] A. Achucarro, J.-O. Gong, S. Hardeman, G. A. Palma, and S. P. Patil, *JCAP* **01**, 030 (2011), arXiv:1010.3693 [hep-ph].
- [27] N. Aghanim *et al.* (Planck), *Astron. Astrophys.* **641**, A6 (2020), [Erratum: Astron.Astrophys. 652, C4 (2021)], arXiv:1807.06209 [astro-ph.CO].
- [28] Y. Akrami *et al.* (Planck), *Astron. Astrophys.* **641**, A10 (2020), arXiv:1807.06211 [astro-ph.CO].
- [29] Y. Akrami *et al.* (Planck), *Astron. Astrophys.* **641**, A9 (2020), arXiv:1905.05697 [astro-ph.CO].
- [30] T. Bringmann, P. Scott, and Y. Akrami, *Phys. Rev. D* **85**, 125027 (2012), arXiv:1110.2484 [astro-ph.CO].
- [31] J. Kristiano and J. Yokoyama, *Phys. Rev. Lett.* **132**, 221003 (2024), arXiv:2211.03395 [hep-th].
- [32] G. Ballesteros and M. Taoso, *Phys. Rev. D* **97**, 023501 (2018), arXiv:1709.05565 [hep-ph].
- [33] M. Braglia, D. K. Hazra, F. Finelli, G. F. Smoot, L. Sriramkumar, and A. A. Starobinsky, *JCAP* **08**, 001 (2020), arXiv:2005.02895 [astro-ph.CO].
- [34] G. A. Palma, S. Sypsas, and C. Zenteno, *Phys. Rev. Lett.* **125**, 121301 (2020), arXiv:2004.06106 [astro-ph.CO].
- [35] G. Ballesteros, J. Rey, M. Taoso, and A. Urbano, *JCAP* **07**, 025 (2020), arXiv:2001.08220 [astro-ph.CO].
- [36] V. Atal, J. Cid, A. Escrivà, and J. Garriga, *JCAP* **05**, 022 (2020), arXiv:1908.11357 [astro-ph.CO].
- [37] S. Pi, Y.-l. Zhang, Q.-G. Huang, and M. Sasaki, *JCAP* **05**, 042 (2018), arXiv:1712.09896 [astro-ph.CO].
- [38] S. Kawai and J. Kim, *Phys. Rev. D* **104**, 083545 (2021), arXiv:2108.01340 [astro-ph.CO].
- [39] J. Lin, Q. Gao, Y. Gong, Y. Lu, C. Zhang, and F. Zhang, *Phys. Rev. D* **101**, 103515 (2020), arXiv:2001.05909 [gr-qc].
- [40] R. Arya, R. K. Jain, and A. K. Mishra, *JCAP* **02**, 034 (2024), arXiv:2302.08940 [astro-ph.CO].

- [41] K. Bamba and S. D. Odintsov, *Symmetry* **7**, 220 (2015), arXiv:1503.00442 [hep-th].
- [42] P.-B. Chen and T.-J. Gao, (2025), arXiv:2501.12242 [astro-ph.CO].
- [43] Z.-Z. Peng, Z.-M. Zeng, C. Fu, and Z.-K. Guo, *Phys. Rev. D* **106**, 124044 (2022), arXiv:2209.10374 [gr-qc].
- [44] M. Y. Khlopov, *Res. Astron. Astrophys.* **10**, 495 (2010), arXiv:0801.0116 [astro-ph].
- [45] B. Carr, F. Kuhnel, and M. Sandstad, *Phys. Rev. D* **94**, 083504 (2016), arXiv:1607.06077 [astro-ph.CO].
- [46] M. Sasaki, T. Suyama, T. Tanaka, and S. Yokoyama, *Class. Quant. Grav.* **35**, 063001 (2018), arXiv:1801.05235 [astro-ph.CO].
- [47] B. Carr and F. Kuhnel, *Ann. Rev. Nucl. Part. Sci.* **70**, 355 (2020), arXiv:2006.02838 [astro-ph.CO].
- [48] V. De Luca, G. Franciolini, and A. Riotto, *Phys. Rev. Lett.* **126**, 041303 (2021), arXiv:2009.08268 [astro-ph.CO].
- [49] I. Musco, *Phys. Rev. D* **100**, 123524 (2019), arXiv:1809.02127 [gr-qc].
- [50] B. Carr, S. Clesse, J. Garcia-Bellido, M. Hawkins, and F. Kuhnel, *Phys. Rept.* **1054**, 1 (2024), arXiv:2306.03903 [astro-ph.CO].
- [51] B. Carr and F. Kuhnel, *SciPost Phys. Lect. Notes* **48**, 1 (2022), arXiv:2110.02821 [astro-ph.CO].
- [52] J. Liu, L. Bian, R.-G. Cai, Z.-K. Guo, and S.-J. Wang, *Phys. Rev. D* **105**, L021303 (2022), arXiv:2106.05637 [astro-ph.CO].
- [53] S. Choudhury, S. Panda, and M. Sami, *JCAP* **11**, 066 (2023), arXiv:2303.06066 [astro-ph.CO].
- [54] Y. Gouttenoire and T. Volansky, *Phys. Rev. D* **110**, 043514 (2024), arXiv:2305.04942 [hep-ph].
- [55] K. M. Belotsky, A. D. Dmitriev, E. A. Esipova, V. A. Gani, A. V. Grobov, M. Y. Khlopov, A. A. Kirillov, S. G. Rubin, and I. V. Svdakovskiy, *Mod. Phys. Lett. A* **29**, 1440005 (2014), arXiv:1410.0203 [astro-ph.CO].
- [56] G. Domènech, *Universe* **7**, 398 (2021), arXiv:2109.01398 [gr-qc].
- [57] S. Mollerach, D. Harari, and S. Matarrese, *Phys. Rev. D* **69**, 063002 (2004), arXiv:astro-ph/0310711.
- [58] K. N. Ananda, C. Clarkson, and D. Wands, *Phys. Rev. D* **75**, 123518 (2007), arXiv:gr-qc/0612013.
- [59] D. Baumann, P. J. Steinhardt, K. Takahashi, and K. Ichiki, *Phys. Rev. D* **76**, 084019 (2007), arXiv:hep-th/0703290.
- [60] G. Agazie *et al.* (NANOGrav), *Astrophys. J. Lett.* **951**, L8 (2023), arXiv:2306.16213 [astro-ph.HE].
- [61] D. J. Reardon *et al.*, *Astrophys. J. Lett.* **951**, L6 (2023), arXiv:2306.16215 [astro-ph.HE].
- [62] J. Antoniadis *et al.* (EPTA, InPTA:), *Astron. Astrophys.* **678**, A50 (2023), arXiv:2306.16214 [astro-ph.HE].
- [63] H. Xu *et al.*, *Res. Astron. Astrophys.* **23**, 075024 (2023), arXiv:2306.16216 [astro-ph.HE].
- [64] A. Afzal *et al.* (NANOGrav), *Astrophys. J. Lett.* **951**, L11 (2023), [Erratum: *Astrophys.J.Lett.* 971, L27 (2024), Erratum: *Astrophys.J.* 971, L27 (2024)], arXiv:2306.16219 [astro-ph.HE].
- [65] D. G. Figueroa, M. Pieroni, A. Ricciardone, and P. Simakachorn, *Phys. Rev. Lett.* **132**, 171002 (2024), arXiv:2307.02399 [astro-ph.CO].
- [66] J. Ellis, M. Fairbairn, G. Franciolini, G. Hütsi, A. Iovino, M. Lewicki, M. Raidal, J. Urrutia, V. Vaskonen, and H. Veermäe, *Phys. Rev. D* **109**, 023522 (2024), arXiv:2308.08546 [astro-ph.CO].
- [67] S.-j. Wang and N. Li, (2025), arXiv:2503.01243 [astro-ph.CO].
- [68] J. Cang, Y. Gao, Y. Liu, and S. Sun, *Phys. Lett. B* **864**, 139429 (2025), arXiv:2309.15069 [astro-ph.CO].
- [69] J.-Z. Zhou, Y.-T. Kuang, Z. Chang, and H. Lü, *Astrophys. J.* **979**, 178 (2025), arXiv:2410.10111 [astro-ph.CO].
- [70] J. Cang, Y.-Z. Ma, and Y. Gao, *Astrophys. J.* **949**, 64 (2023), arXiv:2210.03476 [astro-ph.CO].
- [71] I. Ben-Dayan, B. Keating, D. Leon, and I. Wolfson, *JCAP* **06**, 007 (2019), arXiv:1903.11843 [astro-ph.CO].
- [72] S. Wang, Z.-C. Zhao, and Q.-H. Zhu, *Phys. Rev. Res.* **6**, 013207 (2024), arXiv:2307.03095 [astro-ph.CO].
- [73] P. Auclair *et al.* (LISA Cosmology Working Group), *Living Rev. Rel.* **26**, 5 (2023), arXiv:2204.05434 [astro-ph.CO].
- [74] L. Iacconi, M. Bacchi, L. F. Guimarães, and F. T. Falciano, (2024), arXiv:2412.02544 [astro-ph.CO].
- [75] R. Flauger, N. Karnesis, G. Nardini, M. Pieroni, A. Ricciardone, and J. Torrado, *JCAP* **01**, 059 (2021), arXiv:2009.11845 [astro-ph.CO].
- [76] B. Carr, K. Kohri, Y. Sendouda, and J. Yokoyama, *Rept. Prog. Phys.* **84**, 116902 (2021), arXiv:2002.12778 [astro-ph.CO].
- [77] Z. Yi, Z.-Q. You, Y. Wu, Z.-C. Chen, and L. Liu, *JCAP* **06**, 043 (2024), arXiv:2308.14688 [astro-ph.CO].
- [78] S. Wang, Z.-C. Zhao, J.-P. Li, and Q.-H. Zhu, *Phys. Rev. Res.* **6**, L012060 (2024), arXiv:2307.00572 [astro-ph.CO].
- [79] G. Perna, C. Testini, A. Ricciardone, and S. Matarrese, *JCAP* **05**, 086 (2024), arXiv:2403.06962 [astro-ph.CO].
- [80] T. Papanikolaou, X.-C. He, X.-H. Ma, Y.-F. Cai, E. N. Saridakis, and M. Sasaki, *Phys. Lett. B* **857**, 138997 (2024), arXiv:2403.00660 [astro-ph.CO].
- [81] R.-g. Cai, S. Pi, and M. Sasaki, *Phys. Rev. Lett.* **122**, 201101 (2019), arXiv:1810.11000 [astro-ph.CO].
- [82] K. Kohri and T. Terada, *Phys. Rev. D* **97**, 123532 (2018), arXiv:1804.08577 [gr-qc].
- [83] P. Adshead, K. D. Lozanov, and Z. J. Weiner, *JCAP* **10**, 080 (2021), arXiv:2105.01659 [astro-ph.CO].
- [84] J.-P. Li, S. Wang, Z.-C. Zhao, and K. Kohri, (2025), arXiv:2505.16820 [astro-ph.CO].
- [85] J.-P. Li, S. Wang, Z.-C. Zhao, and K. Kohri, *JCAP* **10**, 056 (2023), arXiv:2305.19950 [astro-ph.CO].
- [86] J.-Z. Zhou, X. Zhang, Q.-H. Zhu, and Z. Chang, *JCAP* **05**, 013 (2022), arXiv:2106.01641 [astro-ph.CO].

- [87] Z. Chang, Y.-T. Kuang, X. Zhang, and J.-Z. Zhou, *Chin. Phys. C* **47**, 055104 (2023), arXiv:2209.12404 [astro-ph.CO].
- [88] D. Wu, J.-Z. Zhou, Y.-T. Kuang, Z.-C. Li, Z. Chang, and Q.-G. Huang, (2024), arXiv:2501.00228 [astro-ph.CO].
- [89] C. Fu, J. Liu, X.-Y. Yang, W.-W. Yu, and Y. Zhang, *Phys. Rev. D* **109**, 063526 (2024), arXiv:2308.15329 [astro-ph.CO].
- [90] M. A. Gorji, M. Sasaki, and T. Suyama, *Phys. Lett. B* **846**, 138214 (2023), arXiv:2307.13109 [astro-ph.CO].
- [91] Z. Chang, Y.-T. Kuang, D. Wu, J.-Z. Zhou, and Q.-H. Zhu, *Phys. Rev. D* **109**, L041303 (2024), arXiv:2311.05102 [astro-ph.CO].
- [92] Z. Chang, Y.-T. Kuang, D. Wu, and J.-Z. Zhou, *JCAP* **2024**, 044 (2024), arXiv:2312.14409 [astro-ph.CO].
- [93] S. Wang, T. Terada, and K. Kohri, *Phys. Rev. D* **99**, 103531 (2019), [Erratum: *Phys. Rev. D* 101, 069901 (2020)], arXiv:1903.05924 [astro-ph.CO].
- [94] K. Saikawa and S. Shirai, *JCAP* **05**, 035 (2018), arXiv:1803.01038 [hep-ph].
- [95] A. Mitridate, D. Wright, R. von Eckardstein, T. Schröder, J. Nay, K. Olum, K. Schmitz, and T. Trickle, (2023), arXiv:2306.16377 [hep-ph].
- [96] W. G. Lamb, S. R. Taylor, and R. van Haasteren, *Phys. Rev. D* **108**, 103019 (2023), arXiv:2303.15442 [astro-ph.HE].
- [97] C. J. Moore and A. Vecchio, *Nature Astron.* **5**, 1268 (2021), arXiv:2104.15130 [astro-ph.CO].
- [98] T. N. Collaboration, “Kde representations of the gravitational wave background free spectra present in the nanograv 15-year dataset,” (2023).
- [99] G. Ashton *et al.*, *Astrophys. J. Suppl.* **241**, 27 (2019), arXiv:1811.02042 [astro-ph.IM].
- [100] J. S. Speagle, *Mon. Not. Roy. Astron. Soc.* **493**, 3132 (2020), arXiv:1904.02180 [astro-ph.IM].
- [101] S. Koposov, J. Speagle, K. Barbary, G. Ashton, E. Bennett, J. Buchner, C. Scheffler, B. Cook, C. Talbot, J. Guillochon, P. Cubillos, A. A. Ramos, M. Dartiaihl, Ilya, E. Tollerud, D. Lang, B. Johnson, jtmendel, E. Higson, T. Vandal, T. Daylan, R. Angus, patelR, P. Cargile, P. Sheehan, M. Pitkin, M. Kirk, J. Leja, joezuntz, and D. Goldstein, “*joshspeagle/dynesty: v2.1.4*,” (2024).
- [102] X. Siemens, J. Ellis, F. Jenet, and J. D. Romano, *Class. Quant. Grav.* **30**, 224015 (2013), arXiv:1305.3196 [astro-ph.IM].
- [103] T. Robson, N. J. Cornish, and C. Liu, *Class. Quant. Grav.* **36**, 105011 (2019), arXiv:1803.01944 [astro-ph.HE].
- [104] S. Hinton, *Journal of Open Source Software* **1**, 45 (2016).
- [105] S. Hinton, S. Dupourqué, J. Zhang, S. wen DENG, , and C. Badger, “*Samreay/chainconsumer: Loosening dependencies*,” (2024).
- [106] D. Wright, J. T. Giblin, and J. Hazboun, (2024), arXiv:2409.15572 [gr-qc].
- [107] T. J. Clarke, E. J. Copeland, and A. Moss, *JCAP* **10**, 002 (2020), arXiv:2004.11396 [astro-ph.CO].
- [108] G. Ferrante, G. Franciolini, A. Iovino, Junior., and A. Urbano, *Phys. Rev. D* **107**, 043520 (2023), arXiv:2211.01728 [astro-ph.CO].
- [109] A. J. Iovino, G. Perna, A. Riotto, and H. Veermäe, *JCAP* **10**, 050 (2024), arXiv:2406.20089 [astro-ph.CO].
- [110] G. Franciolini, A. Iovino, Junior., V. Vaskonen, and H. Veermäe, *Phys. Rev. Lett.* **131**, 201401 (2023), arXiv:2306.17149 [astro-ph.CO].
- [111] I. Musco, V. De Luca, G. Franciolini, and A. Riotto, *Phys. Rev. D* **103**, 063538 (2021), arXiv:2011.03014 [astro-ph.CO].
- [112] I. Musco, K. Jedamzik, and S. Young, *Phys. Rev. D* **109**, 083506 (2024), arXiv:2303.07980 [astro-ph.CO].
- [113] S. Young, *JCAP* **05**, 037 (2022), arXiv:2201.13345 [astro-ph.CO].
- [114] S. Wang, Y.-F. Wang, Q.-G. Huang, and T. G. F. Li, *Phys. Rev. Lett.* **120**, 191102 (2018), arXiv:1610.08725 [astro-ph.CO].
- [115] M. Sasaki, T. Suyama, T. Tanaka, and S. Yokoyama, *Phys. Rev. Lett.* **117**, 061101 (2016), [Erratum: *Phys. Rev. Lett.* 121, 059901 (2018)], arXiv:1603.08338 [astro-ph.CO].
- [116] B. P. Abbott *et al.* (LIGO Scientific, Virgo), *Phys. Rev. Lett.* **121**, 231103 (2018), arXiv:1808.04771 [astro-ph.CO].
- [117] K. Kohri and T. Terada, *Phys. Lett. B* **813**, 136040 (2021), arXiv:2009.11853 [astro-ph.CO].
- [118] S. Babak, A. Petiteau, and M. Hewitson, (2021), arXiv:2108.01167 [astro-ph.IM].
- [119] Z.-Q. You, Z. Yi, and Y. Wu, *JCAP* **11**, 065 (2023), arXiv:2307.04419 [gr-qc].
- [120] C. T. Byrnes, P. S. Cole, and S. P. Patil, *JCAP* **06**, 028 (2019), arXiv:1811.11158 [astro-ph.CO].
- [121] Z.-Z. Peng, C. Fu, J. Liu, Z.-K. Guo, and R.-G. Cai, *JCAP* **10**, 050 (2021), arXiv:2106.11816 [astro-ph.CO].
- [122] Z. Zhou, J. Jiang, Y.-F. Cai, M. Sasaki, and S. Pi, *Phys. Rev. D* **102**, 103527 (2020), arXiv:2010.03537 [astro-ph.CO].
- [123] Y.-F. Cai, X. Tong, D.-G. Wang, and S.-F. Yan, *Phys. Rev. Lett.* **121**, 081306 (2018), arXiv:1805.03639 [astro-ph.CO].
- [124] C. T. Byrnes, E. J. Copeland, and A. M. Green, *Phys. Rev. D* **86**, 043512 (2012), arXiv:1206.4188 [astro-ph.CO].
- [125] V. De Luca, A. Kehagias, and A. Riotto, *Phys. Rev. D* **108**, 063531 (2023), arXiv:2307.13633 [astro-ph.CO].
- [126] T. Nakama and T. Suyama, *Phys. Rev. D* **92**, 121304 (2015), arXiv:1506.05228 [gr-qc].
- [127] Z. Chang, Y.-T. Kuang, X. Zhang, and J.-Z. Zhou, *Universe* **10**, 39 (2024), arXiv:2211.11948 [astro-ph.CO].
- [128] T. Nakama and T. Suyama, *Phys. Rev. D* **94**, 043507 (2016), arXiv:1605.04482 [gr-qc].
- [129] J.-Z. Zhou, Y.-T. Kuang, Z. Chang, X. Zhang, and Q.-H. Zhu, (2023), arXiv:2307.02067 [astro-ph.CO].
- [130] J.-Z. Zhou, Y.-T. Kuang, D. Wu, H. Lü, and Z. Chang, (2024), arXiv:2408.14052 [astro-ph.CO].

- [131] Z.-C. Chen, J. Li, L. Liu, and Z. Yi, *Phys. Rev. D* **109**, L101302 (2024), arXiv:2401.09818 [gr-qc].
- [132] S. Balaji, G. Domènech, and G. Franciolini, *JCAP* **10**, 041 (2023), arXiv:2307.08552 [gr-qc].
- [133] Q.-H. Zhu, Z.-C. Zhao, S. Wang, and X. Zhang, *Chin. Phys. C* **48**, 125105 (2024), arXiv:2307.13574 [astro-ph.CO].
- [134] Z. Chang, X. Zhang, and J.-Z. Zhou, *Phys. Rev. D* **107**, 063510 (2023), arXiv:2209.07693 [astro-ph.CO].
- [135] P. Bari, N. Bartolo, G. Domènech, and S. Matarrese, *Phys. Rev. D* **109**, 023509 (2024), arXiv:2307.05404 [astro-ph.CO].
- [136] Y.-H. Yu and S. Wang, *Eur. Phys. J. C* **84**, 555 (2024), arXiv:2303.03897 [astro-ph.CO].
- [137] R. Picard and M. W. Davies, (2024), arXiv:2410.17819 [astro-ph.CO].
- [138] R. Picard and K. A. Malik, *JCAP* **10**, 010 (2024), arXiv:2311.14513 [astro-ph.CO].
- [139] S. Suga, K. Ichiki, and N. Sugiyama, *Phys. Rev. D* **91**, 024030 (2015), arXiv:1412.1081 [astro-ph.CO].
- [140] X. Zhang, J.-Z. Zhou, and Z. Chang, *Eur. Phys. J. C* **82**, 781 (2022), arXiv:2208.12948 [astro-ph.CO].
- [141] Y.-H. Yu and S. Wang, *Sci. China Phys. Mech. Astron.* **68**, 210412 (2025), arXiv:2405.02960 [astro-ph.CO].
- [142] X.-B. Sui, J. Liu, X.-Y. Yang, and R.-G. Cai, *Phys. Rev. D* **110**, 103541 (2024), arXiv:2407.04220 [astro-ph.CO].